https://dx.doi.org/10.1016/j.ijhydene.2022.03.001

Modelling of Solid Oxide Fuel Cells with Internal Glycerol Steam Reforming

Chen Wang[a], Qijiao He[a], Zheng Li[a], Qidong Xu[a], Minfang Han[b,*], Meng Ni[a,*]

[a] Department of Building and Real Estate, Research Institute for Sustainable Urban Development (RISUD) and Research Institute for Smart Energy (RISE), The Hong Kong Polytechnic University, Hung Hom, Kowloon, Hong Kong, China

[b] Department of Energy and Power Engineering, Tsinghua University, Beijing, Beijing, 100084, China

* *Corresponding author:* hanminfang@tsinghua.edu.cn (M.F. Han); meng.ni@polyu.edu.hk (M. Ni)

Abstract

The direct application of glycerol in solid oxide fuel cell (SOFC) for power generation has been demonstrated experimentally but the detailed mechanisms are not well understood due to the lack of comprehensive modeling study. In this paper, a numerical model is developed to study the glycerol-fueled SOFC. After model validation, the simulated SOFC demonstrates a performance of 7827 $A \cdot m^{-2}$ at 0.6 V, with a glycerol conversion rate of 49% at 1073 K. Then, parametric analyses are conducted to understand the effects of operation conditions on cell performance. It is found that the SOFC performance increases with decreasing operating voltage or increasing inlet temperature. However, increasing either the fuel flow rate or steam to glycerol ratio could decrease the cell performance. It is also interesting to find out that the contribution of H_2 and CO to the total current density is significantly different under various operating conditions, even sometimes CO dominates while H_2 plays a negative role. This is different from our conventional understanding that usually H_2 contributes more significantly to current generation. In addition, cooling measures are needed to ensure the long-term stability of the cell when operating at a high current density.

Keywords: Solid oxide fuel cell; Numerical modeling; Glycerol; Internal reforming; Thermal effect

1 Introduction

The development of clean and efficient power generation technologies is essential to address the global energy consumption issues and the associated environmental problems. Among numerous technologies, solid oxide fuel cell (SOFC) is very promising due to its high efficiency, high fuel flexibility, low pollution and stable operation [1]. One of the main advantages of SOFC is that it offers excellent fuel flexibility and can theoretically be operated on any combustible fuel [2], such as alkanes [2], ammonia [3], methanol [4], ethanol [5], as well as activated carbon [6] and biomass [7]. Among these, methanol and ethanol are regarded as hopeful candidates because they are both liquid and oxygen-rich, with a lower risk of being poisoned and carbon deposition [8].

In addition, glycerol, a byproduct of biodiesel, is an environmentally friendly and renewable chemical with the properties of non-volatility, non-toxicity and chemical stability. The last decade has witnessed a boom in glycerol production as a result of rapid growth in the biodiesel industry, as the weight of the produced glycerol accounts for approximately 10% of the weight of biodiesel. The global glycerol market size is expected to reach USD 3.5 billion by the year of 2027, growing at a compound annual growth rate of 4.0% [11]. Nonetheless, only a small portion of glycerol is purified for use in the food, tobacco, and cosmetic industries, this could further exacerbate the global glycerol oversupply and result in significant waste [12]. However, the high energy density of pure glycerol (6.260 $kWh \cdot L^{-1}$) and its non-toxicity and non-volatility properties make it a very promising energy fuel to replace methanol and ethanol [13][14]. Therefore, the use of SOFC with glycerol internal reforming for power generation is attractive.

Typically, the Ni-based anode may be suffered from carbon deposition when using hydrocarbon fuels in SOFC (Eq. (1), (2) and (3)). The deposited carbon not only blocks the contact of the syngas with the active site and leads to a reduction in catalytic activity, but also

pushes away the nickel particles and causes great damage to the anode structure [2]. The mechanism and possible hazards of carbon deposition have been reported in detail in refs. [15]. As a multi-carbon compound, glycerol is oxygenated although it has C-C bonds, which reduces the possibility of carbon accumulation to some extent.

$$2CO(g) \leftrightarrow CO_2(g)+C(s) \ , \ \Delta H = -171 kJ/mol \quad (1)$$

$$CH_4(g) \leftrightarrow 2H_2(g)+C(s) \ , \ \Delta H = +75 kJ/mol \quad (2)$$

$$CO(g)+H_2(g) \leftrightarrow H_2O(g)+C(s) \ , \ \Delta H = -131 kJ/mol \quad (3)$$

To avoid carbon deposition of glycerol in SOFC, using other metals (Cu [17], Ce [18] and Co [19]) to modify the nickel-based anode or adding basic oxides (La_2O_3 [20], MgO [21] and Al_2O_3 [22]) are good strategies. However, both the complicated process and higher cost impede the commercial application. Apart from developing new anodes, carbon formation can be inhibited by changing the working conditions since the carbon formation reactions (Eq. (1), (2) and (3)) are heavily dependent on the operating parameters. For example, increasing the reaction temperature (facilitating the reversed reactions of (1) and (3) [12,23] or providing sufficient oxygen carrier (e.g., steam) to the glycerol can both inhibit carbon formation. Both Adhikari [12] and Wang [23] found by thermodynamic calculations that carbon deposition of glycerol can be completely suppressed at 1000 K, while the possibility of carbon buildup can be significantly reduced by increasing the amount of inlet steam when the temperature is under 1000 K. Slinn et al. [24] tested the performance of pure glycerol in an electrolyte-supported SOFC with the addition of Pt/Al_2O_3 catalyst and reported steady operation for 30 h. Although a small amount of carbon deposition (0.4% of the feedstock) was observed, it did not cause any adverse effect. Won et al. [25] studied the behavior of a tubular glycerol-fueled SOFC and reported a maximum power density of 265 $mW \cdot cm^{-2}$ at 800 °C, equivalent to 79% of the SOFC performance using hydrogen. Lo Faro et al. [26] used Ni-modified chalcocite and cerium oxide in the SOFC anode to convert glycerol to syngas and achieved 850 $mW \cdot cm^{-2}$ at 0.6 V by using

dry glycerol and found no carbon buildup through long-term testing over 160 hours.

All the above studies demonstrate the feasibility of strategies to suppress the carbon deposition in nickel-based anode SOFC fueled by glycerol. However, the intensity of chemical/electrochemical reactions are highly temperature dependent and increasing the steam flow rate will inevitably dilute the reactant concentration, all of which will lead to complications in fluid-solid coupling, chemical/electrochemical reactions as well as heat transfer processes within the SOFC. Although several experimental studies have been reported on glycerol fueled SOFCs, no modeling approaches have been used to investigate the reforming process and thermodynamics of glycerol inside SOFC. Therefore, in this work, a 2D numerical model is developed to simulate the glycerol steam reforming and electrochemical reactions in a typical tubular SOFC. The output characteristics and temperature distribution under different operating parameters (fuel flow rate and steam to glycerol ratio) and working conditions (inlet temperature and operating voltage) are analyzed through the thermal coupling of the glycerol reforming with electrochemical reactions.

2 Model development

2.1 Physical model

Fig. 1 presents the schematic diagram of an anode-supported tubular SOFC with internal reforming of glycerol. A two-dimensional numerical model is developed to simulate the chemical/electrochemical reactions, electron/ion transfer, mass/momentum transport, and heat transfer processes inside the SOFC. The cell uses Ni-YSZ (yttria-stabilized zirconia) composite as the anode, YSZ as the electrolyte, and YSZ-LSM (lanthanum strontium manganite) composite as the cathode, with thicknesses of 600 μm,10 μm and 100 μm for the anode, electrolyte, and cathode, respectively. The detailed material properties and geometric parameters are shown in Table 1.

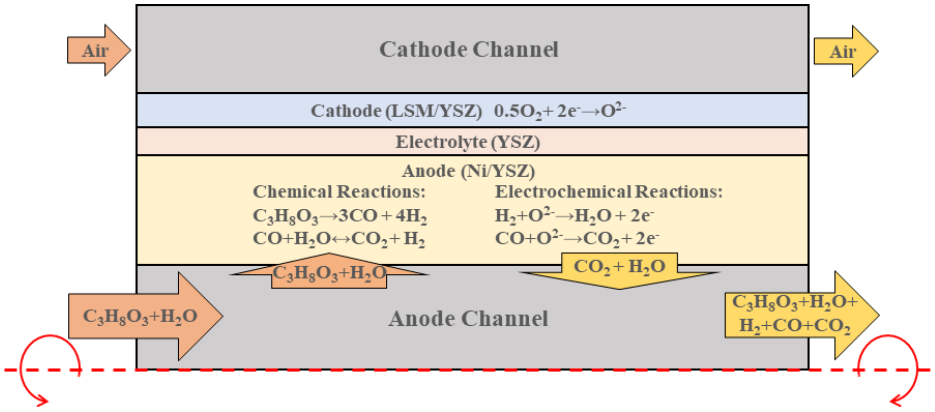

Fig.1 Anode-Supported tubular SOFC

Table 1 Material properties and geometric parameters [40]

Materials or Parameters	Expression or Value	Unit
Electronic conductivity		
Ni	$3.27\times10^{6}-1065.3\times T$	$S\cdot m^{-1}$
LSM	$4.2\times10^{7}/T\times e^{\frac{-1150}{T}}$	$S\cdot m^{-1}$
Ionic conductivity		
YSZ	$3.34\times10^{4}\times e^{\frac{-10300}{T}}$	$S\cdot m^{-1}$
Dimensions		
Cell length	60	mm
Anode channel	2	mm
Cathode channel	2	mm
Anode	600	μm
Cathode	100	μm
Electrolyte	10	μm
Tortuosity	3	-
Porosity		
Anode	0.46	-

Cathode	0.46	-
Permeability		
Anode	1.76×10^{-11}	m^2
Cathode	1.76×10^{-11}	m^2
S_{TPB}		
Anode	1.06×10^{5}	$m^2\cdot m^{-3}$
Cathode	1.33×10^{5}	$m^2\cdot m^{-3}$

During lab testing, glycerol and steam are supplied to the anode channel and a small amount of helium is used as the carrier gas, while air is supplied to the cathode channel. Glycerol and steam will undergo glycerol steam reforming reaction (GSR, Eq. (4)) catalyzed by Ni in the anode. This reaction can proceed in two steps, glycerol decomposition reaction (GDR, Eq. (5)) and water gas shifting reaction (WGSR, Eq. (6)). Although methane can be produced by glycerol decomposition, its formation requires high pressure and relatively low temperature [23], so methane generation and reaction are not favorable and not considered in this study. Although carbon can be formed by side reactions (Eq. (1), (2) and (3)), this can be completely suppressed by controlling the reaction conditions [27]. As no obvious carbon deposition was observed in the experimental studies [25][26], carbon deposition is also not considered. The H_2 and CO produced by GSR will electrochemically react with O^{2-} coming from the cathode at the triple phase boundary (TPB) of anode to form H_2O and CO_2 (Eq. (7), (8)), while the generated electrons are transmitted from anode to cathode through external circuit to react with oxygen to form O^{2-} (Eq. (9)).

$$C_3H_8O_3+3H_2O \rightarrow 3CO_2+7H_2 \ , \ \Delta H=+128\text{kJ/mol} \quad (4)$$

$$C_3H_8O_3 \rightarrow 3CO+4H_2 \ , \ \Delta H=+251\text{kJ/mol} \quad (5)$$

$$CO+H_2O \leftrightarrow CO_2+H_2 \ , \ \Delta H=-41\text{kJ/mol} \quad (6)$$

$$CO+O^{2-} \rightarrow CO_2 \quad (7)$$

$$H_2+O^{2-} \rightarrow H_2O \quad (8)$$

$$0.5O_2+2e^- \rightarrow O^{2-} \quad (9)$$

Based on the above mechanisms, the following assumptions are used in this study:

(1) Only considering electrochemical reactions of H_2 and CO.

(2) Active sites for chemical/electrochemical reactions are uniformly distributed.

(3) The ionic/electronic phase is continuous and homogeneous.

(4) The gases are ideal and incompressible.

(5) Carbon deposition and thermal radiation are not considered.

2.2 Governing equations

Based on the material transfer and reaction processes in SOFC, the 2D model includes the following five sub-models.

2.2.1 Chemical reaction model

The chemical reaction model is used to describe the glycerol steam reforming (GSR) reaction in the anode layer. The internal steam reforming process of glycerol in SOFC is composed of two steps, glycerol decomposition reaction (GDR) and water gas substitution reaction (WGSR). The reaction rates of GDR and WGSR can be obtained as:

GDR [28]:

$$R_{\mathrm{GDR}}=0.036e^{\frac{-63300}{RT}} p_{C_3H_8O_3}^{0.253} p_{H_2O}^{0.358} A_{\text{metal surface}} \quad (10)$$

WGSR [29]:

$$R_{\mathrm{WGSR}}=0.0171e^{\frac{-103196}{RT}} (p_{H_2O}^{l} p_{CO}^{l} - \frac{p_{H_2}^{l} p_{CO_2}^{l}}{K_{ps}}) \quad (11)$$

$$K_{ps} = \exp(-0.2935Z^3 + 0.6351Z^2 + 4.1788Z + 0.3169) \quad (12)$$

$$Z = \frac{1000}{T} - 1 \tag{13}$$

where R is the gas constant; T is temperature, K; $A_{\text{metal surface}}$ is the catalyst's metal surface area, m^2; p_i^l is the partial pressure of specie i, Pa.

2.2.2 Electrochemical reaction model

In this study, H_2 and CO produced by the glycerol steam reforming reaction will participate in electrochemical reactions simultaneously for electron generation (Eq. (7), (8)). The operating potential (V) can be calculated as:

$$V = E - \eta_{\text{act,a}} - \eta_{\text{act,c}} - \eta_{\text{ohmic}} \tag{14}$$

where E represents the thermodynamic equilibrium potential; η_{act} is the activation overpotential; η_{ohmic} is the ohmic overpotential associated with ion/electron conduction.

Since H_2 and CO are both involved in the electrochemical reactions in this study, E can be obtained by [30]:

$$E_{\text{H}_2} = E_{\text{H}_2}^T + \frac{RT}{2F}\left(\frac{p_{\text{H}_2}^l \left(p_{\text{O}_2}^l\right)^{0.5}}{p_{\text{H}_2\text{O}}^l}\right) \tag{15}$$

$$E_{\text{CO}} = E_{\text{CO}}^T + \frac{RT}{2F}\left(\frac{p_{\text{CO}}^l \left(p_{\text{O}_2}^l\right)^{0.5}}{p_{\text{CO}_2}^l}\right) \tag{16}$$

$$E_{\text{H}_2}^T = 1.253 - 0.00024516T \tag{17}$$

$$E_{\text{CO}}^T = 1.46713 - 0.0004527T \tag{18}$$

Generally, the relationship between current density and activation overpotential can be described using the Butler-Volmer (BV) equation:

$$i = i_0\left[\exp\left(\frac{\alpha n F \eta_{act}}{RT}\right) - \exp\left(\frac{-(1-\alpha) n F \eta_{act}}{RT}\right)\right] \tag{19}$$

where i_0 represents exchange current density, $A \cdot m^{-2}$; n is the number of electrons; α is the charge transfer coefficient; F is the Faraday constant.

The exchange current density is related to the fuel properties and reaction conditions, which can be further described as [30]:

$$i_0 = \gamma \exp\left(-\frac{E_{act}}{RT}\right) \tag{20}$$

where γ is pre-expontential factor; E_{act} is the activation energy, J·mol^{-1}. In this case, the pre-expontential factor of H_2 is set to 2.2 times that of CO, and the detailed parameters are shown in [31].

Besides, the ohmic potential losses (η_{ohmic}) can be described according to Ohm's law:

$$i_l = -\sigma_{l,eff} \nabla(\varnothing_l) \tag{21}$$

$$i_s = -\sigma_{s,eff} \nabla(\varnothing_s) \tag{22}$$

where $\varnothing_l$ and $\varnothing_s$ represent the ionic and electronic conduction potentials; $\sigma_{l,eff}$ and $\sigma_{s,eff}$ represent the effective conductivities of ionic and electronic, which are associated with tortuosity and volume fractions of ionic (V_l) and electronic (V_s).

$$\sigma_{l,eff} = \sigma_l \frac{V_l}{\tau_l} \tag{23}$$

$$\sigma_{s,eff} = \sigma_s \frac{V_s}{\tau_s} \tag{24}$$

2.2.3 Fluid flow model

For fluid flow, the momentum transport is described using the classical Navier-Stokes (N-S) equation [32]. For gas channels, N-S equation is given by:

$$\rho \frac{\partial u}{\partial t} + \rho u \nabla u = -\nabla p + \nabla[\mu(\nabla u + (\nabla u)^T) - \frac{2}{3}\mu \nabla u] \tag{25}$$

For porous electrodes, N-S equation containing the Darcy's term is given by:

$$\rho \frac{\partial u}{\partial t} + \rho u \nabla u = -\nabla p + \nabla[\mu(\nabla u + (\nabla u)^T) - \frac{2}{3}\mu \nabla u] - \frac{\varepsilon \mu u}{k} \tag{26}$$

where ρ is density, kg·m^{-3}; μ is dynamic viscosity, kg·m^{-1}·s^{-1}; u is velocity vector, m·s^{-1}; p is

pressure, Pa; ε is porosity; k is permeability of the porous material. And ρ and μ can be calculated by:

$$\rho = \sum_{i=1}^{N} y_i \rho_i \tag{27}$$

$$\mu = \sum_{j=1}^{n} y_i \mu_i \tag{28}$$

where y_i, ρ_i and μ_i are molar friction, density, and dynamic viscosity of specie i, respectively. The dynamic viscosity of each gas can be found in ref. [33].

2.2.4 Mass transfer model

Mass transfer model is used to describe the transfer of various components in SOFC. In this work, the diffusion rate in channels and porous electrodes is described using the general Fick model [35]:

$$N_i = -\frac{1}{RT}\left(\frac{k y_i P}{\mu} \frac{\partial P}{\partial z} - D_{ij,eff} \frac{\partial (y_i P)}{\partial z} \right) \tag{29}$$

where k is permeability; y_i is molar fraction; $D_{ij,eff}$ is the effective binary diffusion coefficient of species i and j by considering molecular diffusion and Knudsen diffusion in the porous electrodes, which can be calculated by [36]:

$$D_{ij,eff} = \frac{\varepsilon}{\tau}\left(\frac{1}{D_{ij}} + \frac{1}{D_{ik}}\right)^{-1} \tag{30}$$

$$D_{ij} = \frac{0.00143 T^{1.75}}{2p\left(v_i^{1/3} + v_j^{1/3}\right)^2}\left(\frac{1}{M_i} + \frac{1}{M_j}\right)^{1/2} \tag{31}$$

$$D_{ik} = \frac{2}{3} r \sqrt{\frac{8RT}{\pi M_i}} \tag{32}$$

where D_{ij} is the binary diffusion coefficient species i and j [37]; D_{ik} is the effective Knudsen diffusion coefficient [38]; v represents the special molecule diffusion volume, which can be found in ref. [39]; r is the radius of electrode pores.

2.2.5 Heat transfer model

In SOFC, the electrochemical reactions at the active sites in TPB generate heat, while the glycerol steam reforming process is highly endothermic. The uneven temperature distribution can seriously affect the performance and stability of the cell. Therefore, the general heat balance equation is used to simulate the heat transfer process [40]:

In channels:

$$\rho c_p \boldsymbol{u} \cdot \nabla T + \nabla \cdot (-\lambda_g \nabla T) = 0 \tag{33}$$

In electrodes and electrolyte:

$$\rho c_p \boldsymbol{u} \cdot \nabla T + \nabla \cdot (-\lambda_{eff} \nabla T) = Q \tag{34}$$

$$\lambda_{eff} = (1-\varepsilon)\lambda_s + \varepsilon\lambda_l \tag{35}$$

where c_p and λ_g represent the heat capacity and thermal conductivity of the gas, respectively; λ_s and λ_l are the solid and liquid phase thermal conductivity, respectively. Q is the heat source term indicating the heat generated or consumed due to chemical/electrochemical reactions and various overpotential losses. The heat sources in this work include heat generation from glycerol steam reforming process, CO and H_2 electrochemical reactions, ohmic losses, and activation losses. The thermodynamic properties of gases and solid materials can be found in ref. [33].

2.3 Model validation

The fuel flow rate, molar fraction, and temperature are specified at the inlet. Constant pressure condition is specified at the outlet. The ends and outer surfaces of the cell are set as adiabatic and insulated. The model is solved by using finite element method.

In order to ensure grid independence, a grid check is conducted (Fig. 2 (a)). It is found that when the number of degrees of freedom reaches 500,000, the relative errors of average current density and total heat are at 0.3% and 1.5% with that of 680,000, so a grid of 500,000 degrees of freedom is used for the subsequent calculation. Meanwhile, the model was validated by

using the experimental results in [25]. The operating conditions in this study can be found in Table 2.

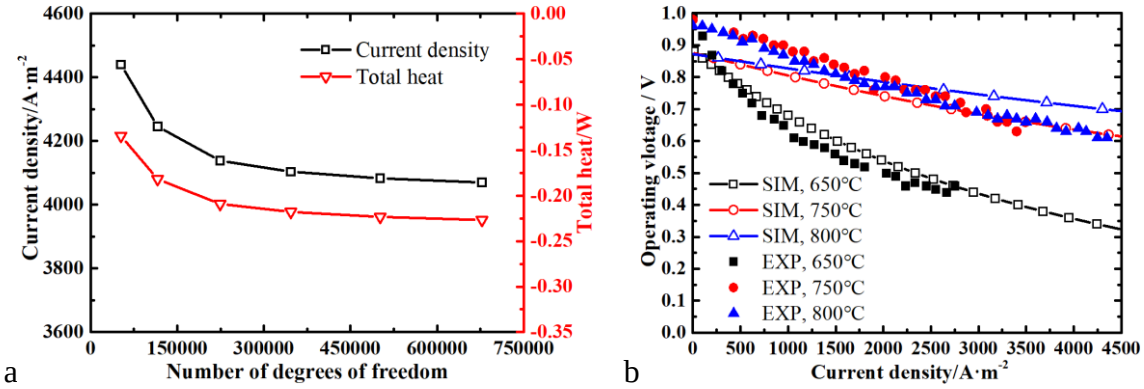

Fig.2 Grid independence (a) and model validation (b)

Table 2 Operating conditions

Parameter	Expression or Value	Unit
Inlet temperature	1023~1123	K
Fuel flow rate*	0.07~0.8	$ml \cdot min^{-1}$
Steam to glycerol ratio (S/G)	1~10	-
Helium flow rate	20	SCCM
Cathode flow rate	500	SCCM
Cathode inlet gas composition	O_2/N_2(molar ratio 21%/79%)	-
Operating potential	0.5~0.8	V
Outlet pressure	1	atm

* As the glycerol fuel is liquid at a room temperature, the unit of $ml.min^{-1}$ is used to quantify the flowrate of the fuel, which is convenient for understanding the consumption of the fuel.

3 Results and discussion

3.1 Effects of operating voltage

The simulation of SOFC with internal glycerol reforming is performed at different operating voltages with an inlet temperature of 1073 K, anode fuel flow rate of 0.139 $ml \cdot min^{-1}$ and steam to glycerol ratio of 3. As expected, the total current density increases from 1643

$A \cdot m^{-2}$ to 12713 $A \cdot m^{-2}$ as the operating voltage decreases from 0.8V to 0.5V, as shown in Fig. 3(a). Besides, the higher electrochemical reaction rate at lower operating voltage results in a faster consumption of fuels (H_2 and CO) and an increase of products (H_2O and CO_2) as shown in Fig. 3(b). The fast consumption of H_2 and CO also facilitates the decomposition of glycerol, resulting in an enhanced glycerol conversion as shown in Fig. 3(b).

From Fig. 3(c) and Fig. 3(d), it is clear that the current density and Nernst potential are unevenly distributed along the flow direction, indicating that the electrochemical reactions inside the cell are highly uneven. It is also noted that when the operating voltage is 0.8V, the current density at the entrance of the cell is negative because the Nernst potential in this region is less than the operating voltage. It indicates that at a high operating voltage, although the cell outputs electrical energy to the outside, not all regions within it play a positive role. This is because the local Nernst potential is lower than the operating voltage in some regions, which consume part of the electrical energy for electrolysis. This phenomenon has also been reported in refs. [41-45].

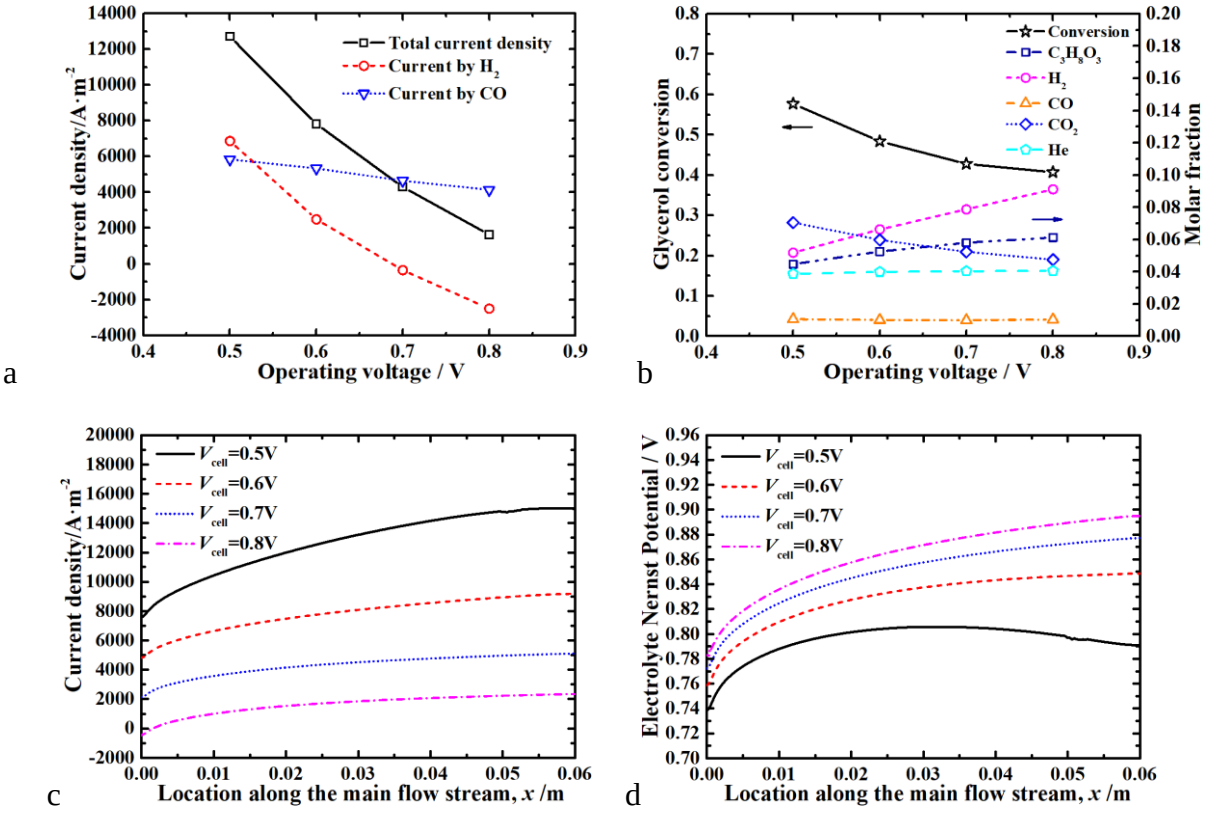

Fig.3 The effects of operating voltage on: (a) current density; (b) molar fraction of gases and glycerol conversion; The distribution of: (c)current density; (d) electrolyte Nernst potential

Besides, the operating voltage plays a role in the internal temperature distribution. Due to the increasing heat production from electrochemical reactions and various overpotential losses, both net heat and average temperature increase with decreasing operating voltage, as shown in Fig. 4(a) and Fig. 4(b). Meanwhile, since the decomposition reaction of glycerol is highly heat-absorbing, the cell reaches thermal-neutrality between 0.6 V and 0.7 V, at which the total heat production of the cell is equivalent to the total heat absorption. However, despite the overall internal thermal balance of the cell, the temperature inside the cell is still unevenly distributed (Fig. 4(c)), with a cooling zone near the inlet and a higher temperature at the outlet. This is mainly due to the higher decomposition rate of glycerol and lower electrochemical reaction rate at the entrance (Fig. 4(d)), resulting in a lower temperature in this region, while the temperature at the outlet is higher due to the local higher electrochemical reaction. Moreover, the temperature unevenness is aggravated at other voltages (Fig. 4(c)), which will result in local performance degradation and large thermal stresses inside the cell [40].

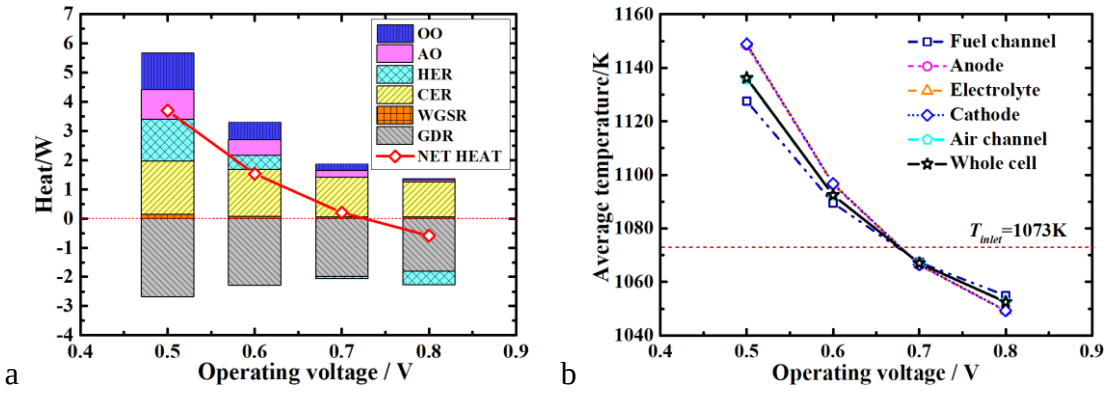

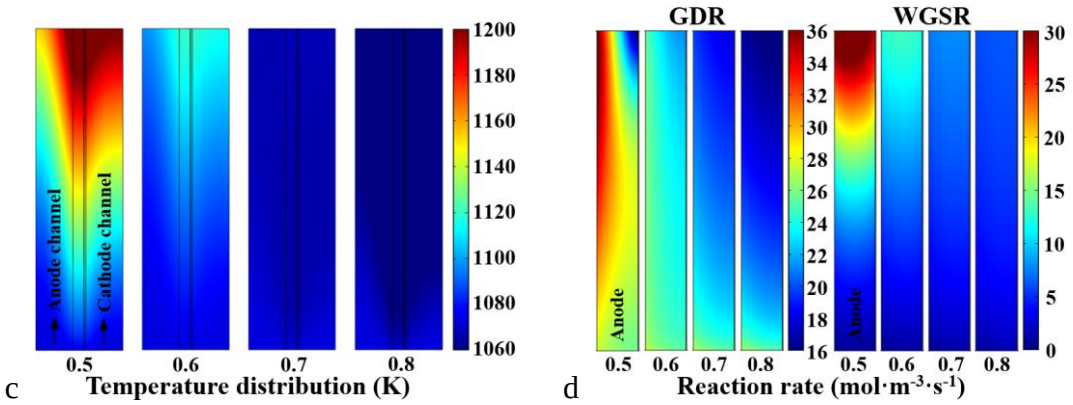

c d

Fig.4 The effects of operating voltage on: (a) heat source; (b) average temperature; (c) temperature distribution; (d) reaction rate

3.2 Effects of fuel flow rate

The simulation is conducted at different fuel flow rates with an inlet temperature of 1073 K, steam to glycerol ratio of 3 and operating voltage of 0.6 V. As shown in Fig. 5(a), increasing anode fuel flow rate decreases the cell performance. As the fuel flow rate increases from 0.07 $ml \cdot min^{-1}$ to $0.8ml \cdot min^{-1}$, the total current density decreases from 8708 $A \cdot m^{-2}$ to 5980 $A \cdot m^{-2}$. This is mainly because the amount of steam will increase proportionally by increasing the fuel flow rate at a fixed steam to glycerol ratio, while the total decomposition of glycerol is not significantly improved (as shown in Fig. 5(b)), which leads to a dilution of H_2 and CO by H_2O in the SOFC, as shown in Fig. 5(c). From Fig. 5(d), it is clear that the current density at the entrance is almost the same under different flow rates, while the dilution effect of steam on the electrochemical reaction becomes more significant along the flow direction.

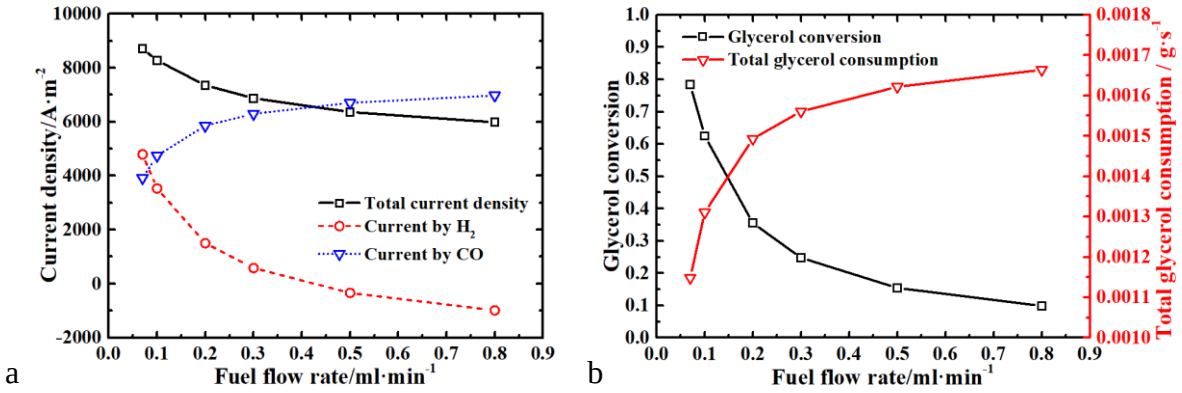

a b

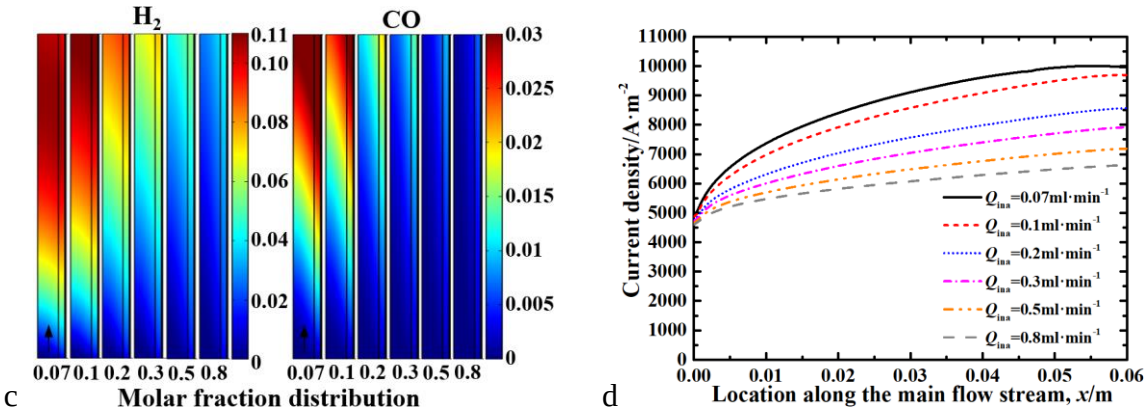

c d

Fig.5 The effects of fuel flow rate on: (a) current density; (b) glycerol conversion and consumption; (c) molar fraction of H_2 and CO; and (d) The distribution of current density

It is also noted from Fig. 5(a) that with increasing fuel flow rate, the current density contributed by CO becomes larger, while that contributed by H_2 gradually decreases and even becomes negative at high flow rates. It indicates that the electrochemical reaction of H_2 becomes weaker while the electrochemical reaction of CO gradually appears to be dominant as the fuel flow rate increases. At high flow rate conditions (e.g., fuel flow rate=0.8ml·min^{-1}), although the cell as a whole generates electricity outward, internally, H_2 is not electrochemically oxidized for current production, instead, H_2O electrolysis consumes part of electricity generated by CO electrochemical oxidation. This is due to the fact that at high flow rates, the large amount of H_2O favors H_2O electrolysis instead of H_2 electrochemical oxidation reaction. For the CO reaction, as more H_2 and CO are produced by glycerol decomposition at high flow rates (Fig. 5(b)), although a large amount of H_2O may dilute CO concentration, more CO can be produced from the internal reforming reaction. Since H_2O electrolysis is favored (H_2 electrochemical oxidation is impeded), the CO electrochemical oxidation becomes a dominating reaction for current generation. As the fuel flow rate increases, more glycerol is consumed, which results in a decrease in the average temperature because the glycerol decomposition reaction is highly heat-absorbing, as shown in Fig. 6(a). Meanwhile, the overall electrochemical reaction is weakened with less electrochemical heat production due to the

dilution effect, resulting in a more uniform temperature distribution, as shown in Fig. 6(b). From Fig. 6(c) and Fig. 6(d), it is clear that the composition of heat sources varies at different flow rates. At small flow rate conditions, the heat absorption of the glycerol decomposition reaction is not significant, and the electrochemical reactions of H_2 and CO are dominant. While at high flow rate conditions, the electrochemical reaction of H_2 is inhibited, whereas the decomposition of glycerol and the electrochemical reaction of CO play the main role.

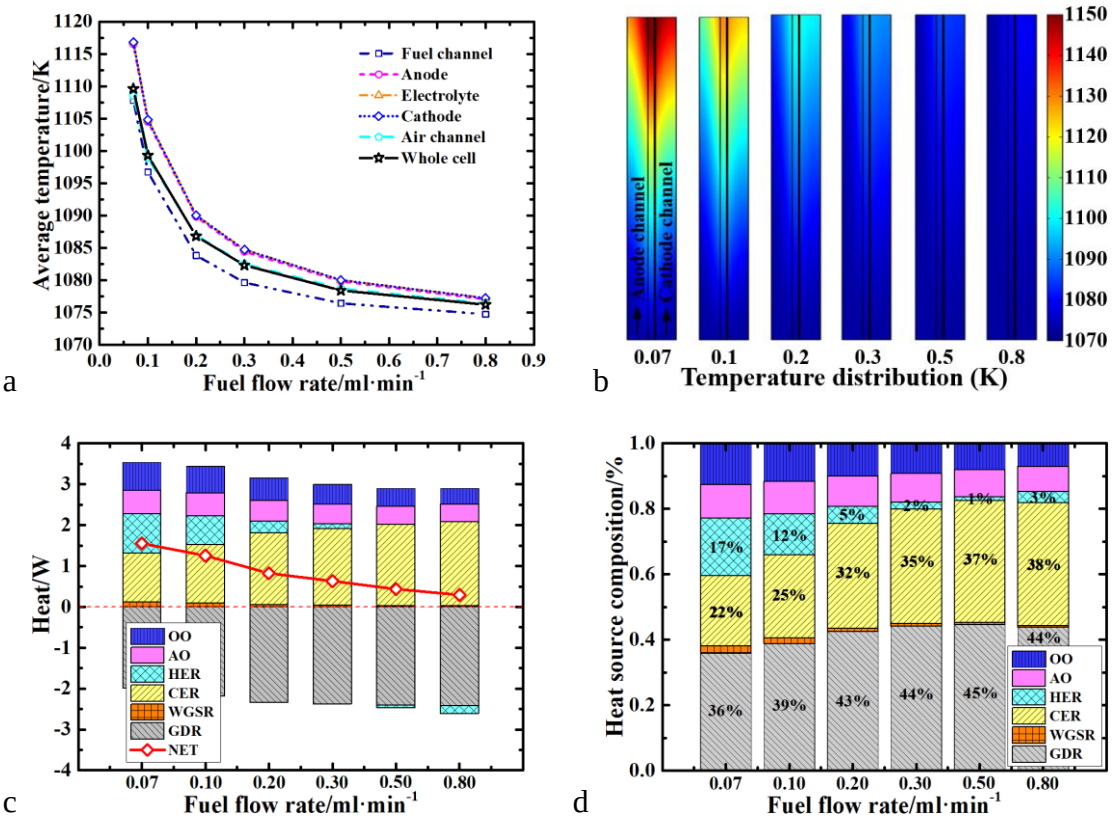

Fig.6 The effects of fuel flow rate on: (a) average temperature; (b) temperature distribution; (c) heat source; (d) heat source composition

3.3 Effects of steam to glycerol ratio

To promote the steam reforming reaction of glycerol and to inhibit carbon deposition, steam is supplied together with glycerol. The simulation is performed at different steam to glycerol ratio (S/G) with an inlet temperature of 1073 K, fuel flow rate of 0.139 ml·min^{-1} and operating voltage of 0.6 V. As shown in Fig. 7(a), the increase of S/G has a negative impact on the output

performance, as the total current density decreases from 9733 $A \cdot m^{-2}$ to 5598 $A \cdot m^{-2}$ when the S/G changes from 1 to 10. This is mainly due to the fact that increasing the steam flow rate at a fixed fuel flow rate will, on the one hand, dilutes the glycerol and reduces its decomposition (Fig. 7(b)), resulting in less H_2 and CO production. On the other hand, it also dilutes the H_2 and CO in the SOFC, leading to a decrease in the current density, as shown in Fig. 7(c). It is also noted from Fig. 7(a) that as S/G increases, the current density contributed by CO increases followed by a slight drop, while that for H_2 shows a decrease. This is due to the fact that increasing the steam flow rate inevitably reduces the production and causes dilution of H_2 and CO, and also inhibits the electrochemical reaction of H_2. While for CO, the strength of its electrochemical reaction is determined by the molar fraction of CO and CO_2, since increasing the steam flow rate dilutes both CO and CO_2. This combined factor determines the electrochemical reaction of CO. From Fig. 7(d), it is clear that the increasing of S/G reduces the current density from the entrance, and this dilution effect becomes more obvious along the main flow.

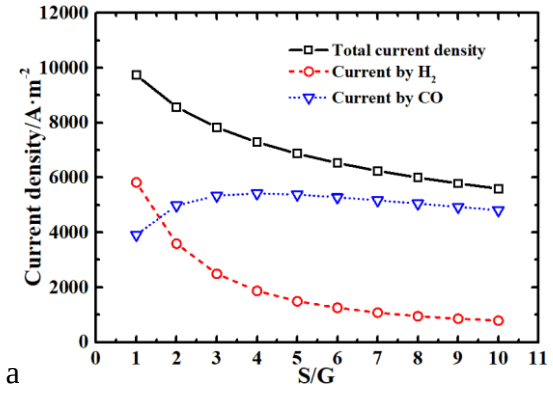

a

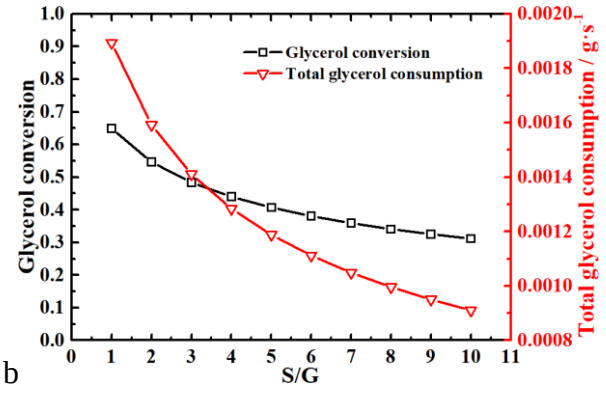

b

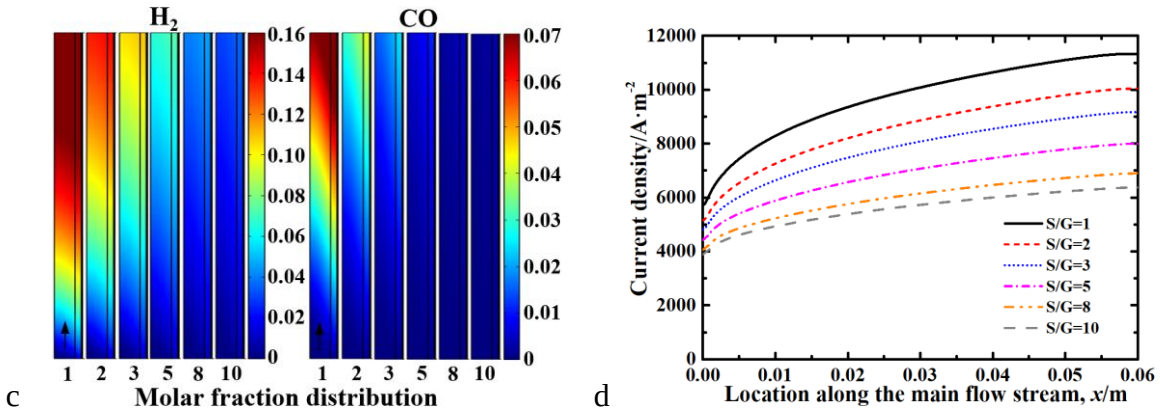

Fig.7 The effects of S/G on: (a) current density; (b) glycerol conversion and consumption; (c) molar fraction of H_2 and CO; and (d) The distribution of current density

Besides, S/G also plays a role in the internal temperature distribution of the cell. As S/G increases, both the net heat and average temperature of the cell decrease, as shown in Fig. 8(a) and Fig. 8(c). This is mainly because the steam dilutes all the substances inside the cell, weakening the decomposition of glycerol and the electrochemical reaction of H_2, both of which absorb/generate less heat. While the enhancement of CO electrochemical reaction is the result of the combined effect of CO and CO_2, making CO electrochemical reaction the main heating source at a larger S/G, as shown in Fig. 8(c) and Fig. 8(d). The smaller heat absorption/production at high S/G results in a more uniform temperature distribution inside the cell (Fig. 8(b)), which enhances the stability of the cell.

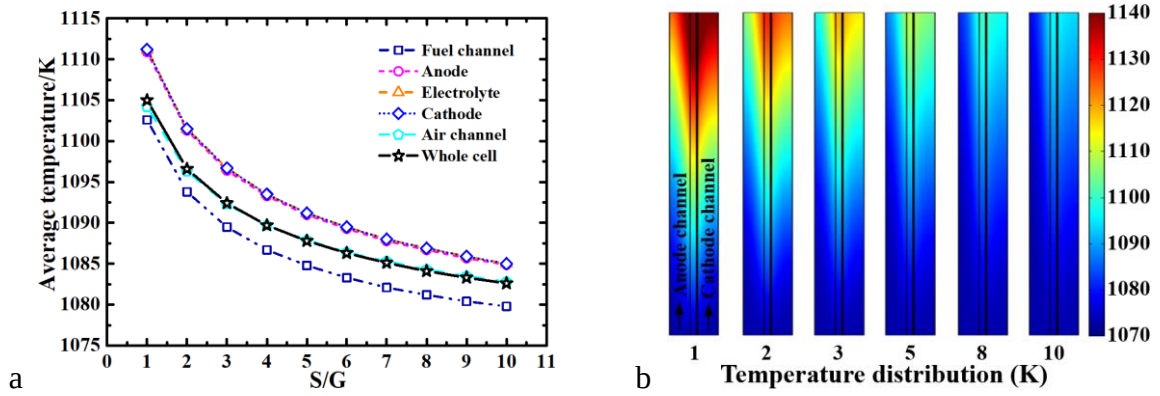

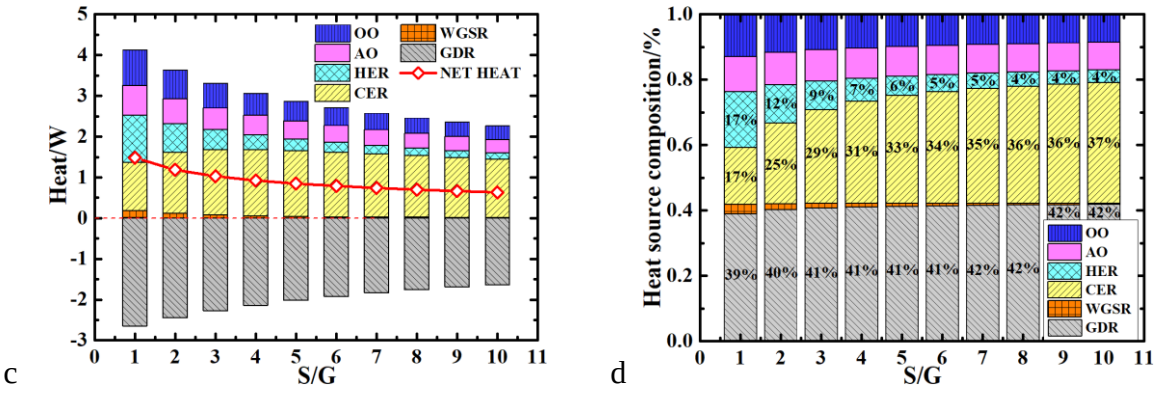

Fig.8 The effects of S/G on: (a) average temperature; (b) temperature distribution; (c) heat source; (d) heat source composition

3.4 Effects of inlet temperature

The inlet temperature affects not only the intensity of chemical/electrochemical reactions but also the thermal properties of the material and gases. The simulation is performed at different inlet temperatures at an operating voltage of 0.6 V, anode fuel flow rate of 0.139 $ml \cdot min^{-1}$ and steam to glycerol ratio of 3. As expected, the inlet temperature has a significant positive effect on the electrochemical performance of the cell, with the total current density increasing from 4847 $A \cdot m^{-2}$ to 11618 $A \cdot m^{-2}$ as the inlet temperature changing from 1023 K to 1123 K. The current density contributed by CO increases from 4286 $A \cdot m^{-2}$ to 5560 $A \cdot m^{-2}$ and that by H_2 increases from 561 $A \cdot m^{-2}$ to 6058 $A \cdot m^{-2}$, as shown in Fig. 9(a). This is because at lower temperatures, the weak decomposition of glycerol (Fig. 9(b)) consumes only a small amount of H_2O (Fig. 9(c)), while the remaining excess H_2O not only dilutes the syngas inside the SOFC, but also significantly inhibits the electrochemical oxidation of H_2. Whereas under high temperature conditions, the rapid decomposition of glycerol produces more syngas on the one hand (Fig. 9(d)) and reduces the quantity of water inside the SOFC on the other hand, thus enhancing the electrochemical reaction of H_2 and CO. It can be seen that CO maintains a high current density over a wide temperature range, while the large increase in H_2 current density indicates that the electrochemical reaction of H_2 is more suitable for high temperature

conditions. Therefore, from the fuel utilization point of view, the SOFC with internal reforming of glycerol is more suitable for operation at high temperature conditions.

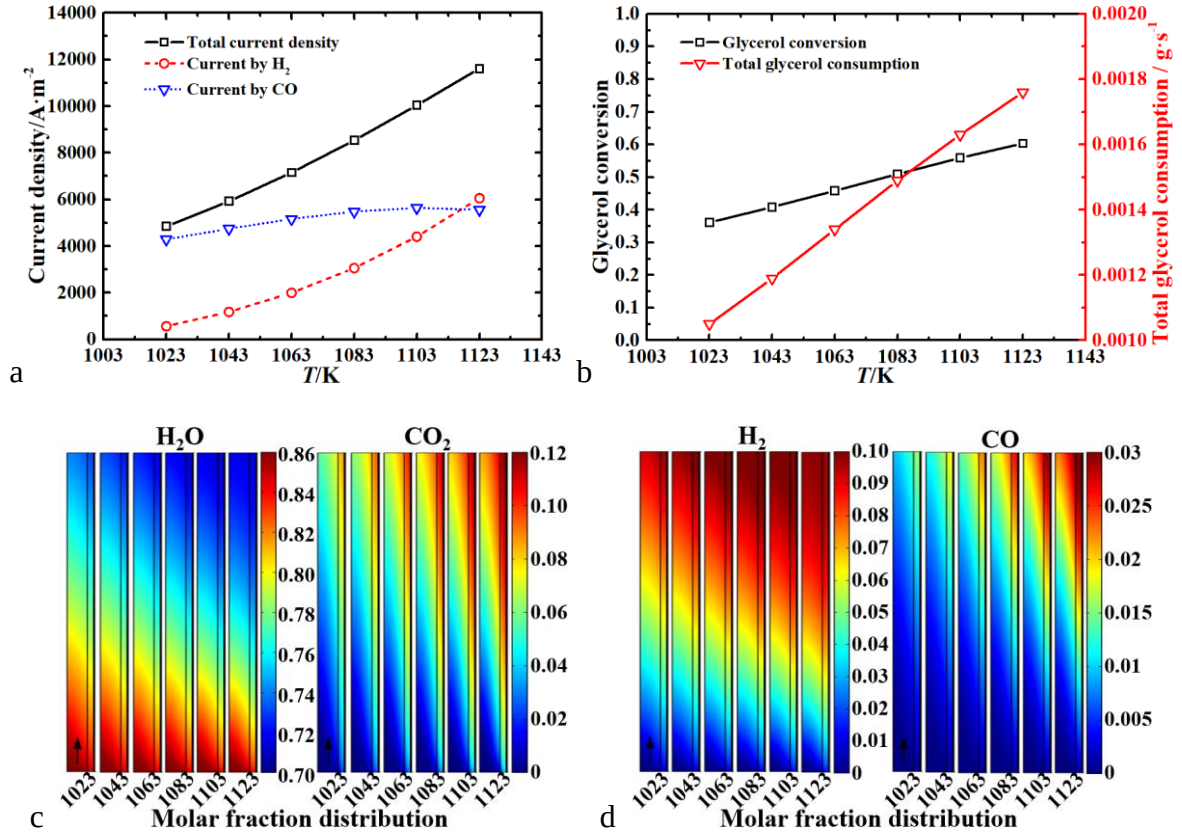

Fig.9 The effects of inlet temperature on: (a) current density; (b) glycerol conversion and consumption; (c) molar fraction of H_2O and CO_2; (d) molar fraction of H_2 and CO

Besides, when the temperature increases, the decomposition reaction of glycerol is enhanced as it is highly heat-absorbing, and the high temperature has a remarkable promotion on the electrochemical reactions of H_2 and CO, causing more heat generation at high temperature, as shown in Fig. 10(a). Moreover, the electrochemical reactions of H_2 are significantly enhanced at high temperatures, thus the electrochemical oxidation of H_2 also becomes the main source of heat production at this time, as shown in Fig. 10(b).

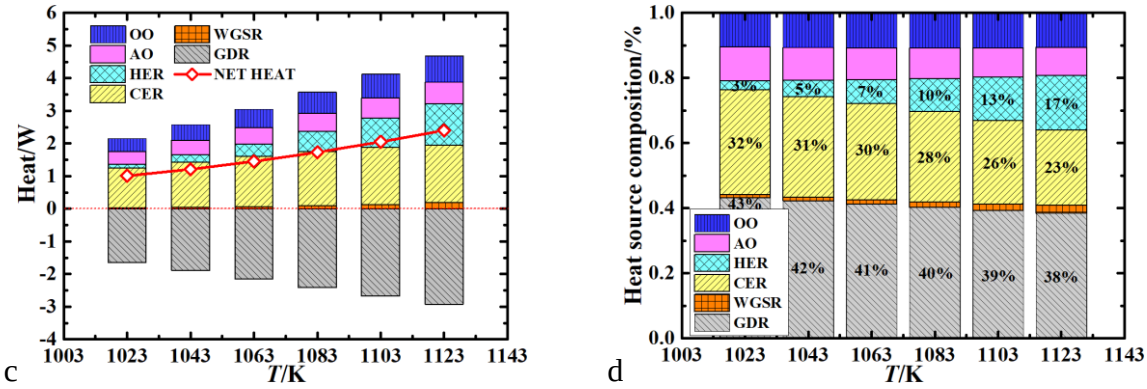

Fig.10 The effects of inlet temperature on: (a) heat source; (b) heat source composition

4 Conclusion

A 2D multi-physics field model is developed to study the output performance and temperature distribution of SOFC with internal glycerol steam reforming. The model fully considers the chemical/electrochemical reactions, fluid-solid coupling, ion/electron transfer and heat transfer processes within the SOFC. The effects of different operating parameters, including operating voltage, fuel flow rate, steam to glycerol ratio as well as inlet temperature, on the output performance and temperature distribution are analyzed.

It is found that reducing the operating voltage or increasing the inlet temperature will promote the electrochemical reaction of H_2 and CO as well as increase the conversion of glycerol, resulting in a higher power output of the cell. Whereas increasing the fuel flow rate or steam to glycerol ratio will both dilute the glycerol and syngas and inhibit the electrochemical reaction of H_2, bringing negative impact on the output performance. It is worth mentioning that the contribution of H_2 and CO to the total current density is significantly different under various operating conditions. The contribution of CO is not as small as expected, but rather under some conditions (high operating voltage or fuel flow rate), it is CO that dominates, while H_2 may consume part of the electrical energy for electrolysis and play a negative role. Finally, it is noted that the increased cell output performance is always accompanied by an extremely uneven temperature distribution. Therefore, for SOFC with

internal glycerol reforming, appropriate cooling strategies are required to improve long-term stability if the cell keeps running in high performance mode.

Overall, this study offers insight into the SOFC with internal glycerol reforming, which is beneficial to promote the development and optimization of glycerol-fueled SOFC.

Acknowledgement

M.F. Han thanks to the grant (NSFC 5201101243) from National Natural Science Foundation of China. M. NI thanks to the grants (Project Number: PolyU 152064/18E and N_PolyU552/20) from Research Grant Council, University Grants Committee, Hong Kong SAR.

Reference

[1] Hoogers G. Fuel cell technology handbook[M]. CRC press, 2002.

[2] McIntosh S, Gorte RJ. Direct hydrocarbon solid oxide fuel cells[J]. Chemical reviews, 2004, 104(10): 4845-4866.

[3] Cinti G, Desideri U, Penchini D, et al. Experimental analysis of SOFC fuelled by ammonia[J]. Fuel Cells, 2014, 14(2): 221-230.

[4] Jiang Y, Virkar AV. A high performance, anode-supported solid oxide fuel cell operating on direct alcohol[J]. Journal of the Electrochemical Society, 2001, 148(7): A706.

[5] Badwal SPS, Giddey S, Kulkarni A, et al. Direct ethanol fuel cells for transport and stationary applications–A comprehensive review[J]. Applied Energy, 2015, 145: 80-103.

[6] Bai YH, Liu Y, Tang YB, et al. Direct carbon solid oxide fuel cell—a potential high

performance battery[J]. international journal of hydrogen energy, 2011, 36(15): 9189-9194.

[7] Radenahmad N, Azad AT, Saghir M, et al. A review on biomass derived syngas for SOFC based combined heat and power application[J]. Renewable and Sustainable Energy Reviews, 2020, 119: 109560.

[8] Cimenti M, Hill JM. Importance of pyrolysis and catalytic decomposition for the direct utilization of methanol in solid oxide fuel cells[J]. Journal of Power Sources, 2010, 195(1): 54-61.

[9] Cimenti M, Hill JM. Direct utilization of liquid fuels in SOFC for portable applications: challenges for the selection of alternative anodes[J]. Energies, 2009, 2(2): 377-410.

[10] Cimenti M, Hill JM. Thermodynamic analysis of solid oxide fuel cells operated with methanol and ethanol under direct utilization, steam reforming, dry reforming or partial oxidation conditions[J]. Journal of Power Sources, 2009, 186(2): 377-384.

[11] Bhatia L. Glycerol and its derivatives (propanediol, glycerolcarbonate, epichlorohydrin): implicit role in bioeconomy[M]//Production of Top 12 Biochemicals Selected by USDOE from Renewable Resources. Elsevier, 2022: 317-343.

[12] Adhikari S, Fernando S, Gwaltney SR, et al. A thermodynamic analysis of hydrogen production by steam reforming of glycerol[J]. International Journal of Hydrogen Energy, 2007, 32(14): 2875-2880.

[13] Arechederra RL, Treu BL, Minteer SD. Development of glycerol/O2 biofuel cell[J]. Journal of Power Sources, 2007, 173(1): 156-161.

[14] Yahya N, Kamarudin SK, Karim NA. Direct glycerol fuel cells (DGFCs)[M]//Direct Liquid Fuel Cells. Academic Press, 2021: 115-136.

[15] Wang W, Su C, Wu YZ, et al. Progress in solid oxide fuel cells with nickel-based anodes operating on methane and related fuels[J]. Chemical reviews, 2013, 113(10): 8104-8151.

[16] Xiao J, Xie YM, Liu J, et al. Deactivation of nickel-based anode in solid oxide fuel cells

operated on carbon-containing fuels[J]. Journal of Power Sources, 2014, 268: 508-516.

[17] Wang C, Dou BL, Chen HS, et al. Renewable hydrogen production from steam reforming of glycerol by Ni–Cu–Al, Ni–Cu–Mg, Ni–Mg catalysts[J]. International journal of hydrogen energy, 2013, 38(9): 3562-3571.

[18] Go YJ, Go GS, Lee HJ, et al. The relation between carbon deposition and hydrogen production in glycerol steam reforming[J]. International Journal of Hydrogen Energy, 2015, 40(35): 11840-11847.

[19] Cheng CK, Foo SY, Adesina AA. Carbon deposition on bimetallic Co–Ni/Al2O3 catalyst during steam reforming of glycerol[J]. Catalysis Today, 2011, 164(1): 268-274.

[20] Hirai T, Ikenaga N, Miyake T, et al. Production of hydrogen by steam reforming of glycerin on ruthenium catalyst[J]. Energy & Fuels, 2005, 19(4): 1761-1762.

[21] Thyssen VV, Georgetti F, Assaf EM. Influence of MgO content as an additive on the performance of Ni/MgOSiO2 catalysts for the steam reforming of glycerol[J]. International Journal of Hydrogen Energy, 2017, 42(27): 16979-16990.

[22] Adhikari S, Fernando S, Haryanto A. Production of hydrogen by steam reforming of glycerin over alumina-supported metal catalysts[J]. Catalysis Today, 2007, 129(3-4): 355-364.

[23] Wang H, Wang XD, Li MS, et al. Thermodynamic analysis of hydrogen production from glycerol autothermal reforming[J]. International Journal of Hydrogen Energy, 2009, 34(14): 5683-5690.

[24] Slinn M, Kendall K, Mallon C, et al. Steam reforming of biodiesel by-product to make renewable hydrogen[J]. Bioresource technology, 2008, 99(13): 5851-5858.

[25] Won JY, Sohn HJ, Song RH, et al. Glycerol as a Bioderived Sustainable Fuel for Solid-Oxide Fuel Cells with Internal Reforming[J]. ChemSusChem: Chemistry & Sustainability Energy & Materials, 2009, 2(11): 1028-1031.

[26] Lo Faro M, Oliveira VL, Reis RM, et al. Solid Oxide Fuel Cell fed directly with dry glycerol[J]. Energy Technology, 2019, 7(1): 45-47.

[27] Adhikari S, Fernando S, Gwaltney SR, et al. A thermodynamic analysis of hydrogen production by steam reforming of glycerol[J]. International Journal of Hydrogen Energy, 2007, 32(14): 2875-2880.

[28] Cheng CK, Foo SY, Adesina AA. Glycerol steam reforming over bimetallic Co−Ni/Al2O3[J]. Industrial & Engineering Chemistry Research, 2010, 49(21): 10804-10817.

[29] Haberman BA, Young JB. Three-dimensional simulation of chemically reacting gas flows in the porous support structure of an integrated-planar solid oxide fuel cell[J]. International Journal of Heat and Mass Transfer, 2004, 47(17-18): 3617-3629.

[30] He QJ, Yu J, Xu HR, et al. Thermal effects in H2O and CO2 assisted direct carbon solid oxide fuel cells[J]. International Journal of Hydrogen Energy, 2020, 45(22): 12459-12475.

[31] Xu HR, Chen B, Tan P, et al. Modeling of all-porous solid oxide fuel cells with a focus on the electrolyte porosity design[J]. Applied Energy, 2019, 235: 602-611.

[32] Xu HR, Chen B, Liu J, et al. Modeling of direct carbon solid oxide fuel cell for CO and electricity cogeneration[J]. Applied Energy, 2016, 178: 353-362.

[33] Coker AK. Ludwig's applied process design for chemical and petrochemical plants[M]. gulf professional publishing, 2014.

[34] LIU QG, MA LX, LIU J. Handbook of Chemistry and Chemical Properties Data (Organic Volume) [M]. Beijing: Chemical Industry Press, 2002: 242.

[35] Suwanwarangkul R, Croiset E, Fowler MW, et al. Performance comparison of Fick's, dusty-gas and Stefan–Maxwell models to predict the concentration overpotential of a SOFC anode[J]. Journal of Power Sources, 2003, 122(1): 9-18.

[36] Veldsink JW, Van Damme RMJ, Versteeg GF, et al. The use of the dusty-gas model for the description of mass transport with chemical reaction in porous media[J]. Chemical

Engineering Journal-Including Biochemical Engineering Journal, 1995, 57(2): 115-126.

[37] Todd B, Young JB. Thermodynamic and transport properties of gases for use in solid oxide fuel cell modelling[J]. Journal of power Sources, 2002, 110(1): 186-200.

[38] Poling BE, Prausnitz JM, O'Connell JP, Reid RC, Sherwood TK, Street RE. The properties of gases and liquids. vol. 12. 2001. doi: 10.1063/1.3060771.

[39] Fuller EN, Ensley K, Giddings JC. Diffusion of halogenated hydrocarbons in helium. The effect of structure on collision cross sections[J]. The Journal of Physical Chemistry, 1969, 73(11): 3679-3685.

[40] Xu QD, Xia LC, He QJ, et al. Thermo-electrochemical modelling of high temperature methanol-fuelled solid oxide fuel cells[J]. Applied Energy, 2021, 291: 116832.

[41] Ye Q, Zhao TS, Yang H, et al. Electrochemical reactions in a DMFC under open-circuit conditions[J]. Electrochemical and Solid State Letters, 2004, 8(1): A52.

[42] Ye Q, Zhao TS. Electrolytic hydrogen evolution in DMFCs induced by oxygen interruptions and its effect on cell performance[J]. Electrochemical and Solid State Letters, 2005, 8(4): A211.

[43] Ye Q, Zhao TS. Abrupt decline in the open-circuit voltage of direct methanol fuel cells at critical oxygen feed rate[J]. Journal of the Electrochemical Society, 2005, 152(11): A2238.

[44] Ye Q, Zhao TS, Liu JG. Effect of Transient Hydrogen Evolution/Oxidation Reactions on the OCV of Direct Methanol Fuel Cells[J]. Electrochemical and Solid State Letters, 2005, 8(10): A549.

[45] Ni M. Electrolytic effect in solid oxide fuel cells running on steam/methane mixture[J]. Journal of Power Sources, 2011, 196(4): 2027-2036.